


# Improved Oxidation Resistance of a New Aluminum-Containing Austenitic Stainless Steel at 800 °C in Air

Yongfeng Qiao<sup>1,2</sup>  · Jian Wang<sup>1,2</sup> · Zhuxia Zhang<sup>2</sup> ·  
Xin Quan<sup>1,2</sup> · Jie Liu<sup>3</sup> · Xudong Fang<sup>4</sup> ·  
Peide Han<sup>1,2</sup>

Received: 17 January 2017 / Published online: 7 February 2017  
© Springer Science+Business Media New York 2017

**Abstract** The oxidation resistance of austenitic stainless steels modified with various aluminum contents was investigated. The weight gain per unit area is in parabolic relation to oxidation time, and the oxidation rate significantly decreases with increased aluminum content. Outer layer oxides of austenitic stainless steel transform from  $\text{Cr}_2\text{O}_3$  to a composite oxide layer comprising Cr and Al, and more dense Al-containing oxides formed with increasing the added Al contents. Since the diffusion of element Al is enhanced and the diffusion of element Cr is inhibited, the oxides enriched in Al dramatically contribute to the improved oxidation resistance of austenitic stainless steels at high temperature. The possible oxidation mechanisms are also proposed based on microstructural observations.

**Keywords** Oxidation · Austenitic stainless steel · Surface · Aluminum

---

✉ Jian Wang  
jianwang1@126.com

✉ Peide Han  
hanpeide@126.com

Yongfeng Qiao  
qiaotyut@126.com

- <sup>1</sup> Key Laboratory of Interface Science and Engineering in Advanced Materials, Taiyuan University of Technology, Ministry of Education, Taiyuan 030024, China
- <sup>2</sup> College of Materials Science and Engineering, Taiyuan University of Technology, No. 79, Yingze Street, Wanbolin District, Taiyuan 030024, China
- <sup>3</sup> College of Materials Science and Engineering, Taiyuan University of Science and Technology, No. 66, Waliu Street, Taiyuan 030024, China
- <sup>4</sup> Taiyuan Iron & Steel Co., Ltd., Taiyuan 030003, China

## Introduction

Due to the increasing energy shortage and environment pollution problems, the development of efficient coal-fired power plants has been a hot topic in recent years [1–3]. In order to improve the efficiency of the thermal power generation, the steam parameters of plant have been increased from supercritical to ultra-supercritical (USC) condition [4–6]. However, with the increase in steam parameters, the materials applied in USC boiler units should offer excellent high-temperature performance. Some new heat-resistant steels, austenitic stainless steels (such as super 304H, TP347HFG, HR3C, etc.), have been synthesized to meet the materials used in the ultra-supercritical boiler units [6–10].

In particular, due to their favorable high-temperature oxidation resistance and excellent creep resistance, good mechanical strength and competitive low cost, the austenitic heat-resistance steels have been extensively used in many industrial fields, ranging from energy-conversion systems to petrochemical factory. The HR3C steel, 25Cr–20Ni-type austenitic heat-resistance steel, has been the preferred candidate materials for the heat exchangers and reactor pressure vessels [11, 12]. Generally, the high-temperature oxidation of the conventional austenitic stainless steels relies on the chromium-containing oxides scales formed on the surface. However, the oxidation resistance of HR3C mainly depends on the formation of a  $\text{Cr}_2\text{O}_3$ -based protective scale, which is unstable at the high-temperature water-steam environment to form volatile Cr oxy-hydroxide species, leading to the breakdown of the protective scales and eventually cause failure of the steels [13–17]. Due to the better thermodynamics stability, the  $\text{Al}_2\text{O}_3$  was usually cooperated with  $\text{Cr}_2\text{O}_3$  to produce protective scales on the surface of the steels and to improve the oxidation resistance [18, 19].

In the past decades, it has been proved that Al addition into the Ni–Cr–W–Mo alloys, 429 ferritic stainless steel and 9–15Cr (wt%) ferritic stainless steels promoted the formation of a continuous Al-containing oxides layer which acts as an excellent diffusion barrier [20–23]. Recently, the alumina-forming austenitic (AFA) stainless steels have also been developed and found to service in harsh environments. The most representative research was the developed creep-resistant AFA stainless steels by the Oak Ridge National Laboratory (ORNL) [24]. These newer grades of AFA alloys have a broad composition range of Fe–(12–35)Ni–(12–15)Cr–(2.5–4)Al–(0.6–3)Nb based on the weight percent (wt%), and the balanced levels of alloying additions, primarily Al, Cr, Mn and Ni, maintain a single austenitic matrix. Meanwhile, the high-temperature ultrafine precipitates like MC or  $\gamma'$ - $\text{Ni}_3\text{Al}$  provide the creep-strengthened effect. Subsequently, Lu et al. [25, 26] also confirmed a new AFA stainless steel with via alloying 3.0 wt% Al based on the NF709 alloys. They found that the stable and exclusive alumina scale was formed in either dry air or air with 10% water vapor mixed environment at 800 °C, which results in the AFA steels that exhibit a good high-temperature oxidation resistance and creep strength. It is believed that the concept for the AFA steels could also be applied to other types of austenitic stainless steel systems, and it is also interesting to develop the AFA steels based on different commercial stainless steels. Therefore,

in recent years, numerous investigations have been conducted regarding the Fe–(12–35)Ni–(12–15)Cr–(2.5–4)Al alloys. It is well inferred from existing investigations that only a few studies have been conducted about the microstructure, mechanical and corrosion properties of AFA with new composition at ultra-supercritical condition.

In the present work, a new austenitic stainless steel based on the composition of Fe–22Cr–25Ni steel has been obtained by introducing the Al element. The oxidation kinetics was studied under high-temperature environment, and the morphology, structure and composition of oxidation layer were researched. An Al-containing compact oxide film can be formed on the AFA steels, leading to the improved oxidation resistance of the austenitic stainless steels. The formation mechanism of the oxide film was proposed as well.

## Experimental Procedures

### Material Preparation

In our study, the experimental alloy with different amounts of Al (1.5, 2.5 and 3.5 wt%) was prepared based on the composition of the 22Cr–25Ni (wt%) steels [27], such as 22Cr–25Ni–1.5Al, 22Cr–25Ni–2.5Al and 22Cr–25Ni–3.5Al, respectively. The HR3C steel (25Cr–20Ni) smelted by TISCO was selected as a reference material. The chemical compositions of austenitic stainless steels containing Al and HR3C are shown in Table 1. Ingots of each given composition were prepared in a 50-kg vacuum induction furnace using commercially pure elements. After melting and casting, the ingots were hot rolled to slab with a thickness of 20 mm. The alloys were eventually solution-treated at 1260 °C and subsequently water-quenched to eliminate precipitation of the second phase.

### High-Temperature Oxidation Testing

The materials were cut using the electrical discharge machining (EDM) technique to yield square test coupon geometry of 15 mm × 13 mm × 3 mm in this work. Prior to the oxidation tests, all the specimens were carefully ground with SiC paper on all sides up to 1200 grit and then cleaned in ethanol by an ultrasonic bath to degrease

**Table 1** Chemical composition of the tested (wt%)

Alloy	Cr	Ni	Al	Nb	Mn	Cu	Si	C	N	Fe
22Cr–25Ni–1.5Al	22.00	25.00	1.50	0.45	0.80	2.75	0.20	0.06	–	Bal
22Cr–25Ni–2.5Al	22.00	25.00	2.50	0.45	0.80	2.75	0.20	0.06	–	Bal
22Cr–25Ni–3.5Al	22.00	25.00	3.50	0.45	0.80	2.75	0.20	0.06	–	Bal
HR3C	24.64	19.42	–	0.37	1.44	0.04	0.38	0.06	0.28	Bal

the surfaces. Isothermal oxidation tests were carried out at 800 °C in the laboratory air for different times. The specimens were put in individual alumina crucibles to collect the spalled oxide. After exposure to the designated temperature for a given duration, the alumina crucibles together with specimens were removed from the furnace and cooled in air with an estimated cooling time of approximately 30 min to room temperature. Gravimetric analysis was used to determine the oxidation behavior of the materials. The single weight of the tested sample, the total weight of both “sample and alumina crucible” before and after exposure were measured using an electronic balance with an accuracy of 0.1 mg. The oxidized samples were embedded in bakelite in order to protect the oxide scale formed, ground with SiC abrasive papers from No. 100 to 2000 and then polished mechanically using 1 and 0.3 μm alumina suspension for cross-sectional investigations.

## Characterizations

The initial microstructures were observed by optical microscopy (OM), before the specimens were etched in the mixed solutions of FeCl<sub>3</sub>:HCl:H<sub>2</sub>O = 5 g:15 ml:60 ml. The surface and cross-sectional morphologies of the specimens after oxidation were analyzed using an MIRA3 TESCAN scanning electron microscope (SEM) equipped with energy-dispersive spectrometer (EDS). The constituent phases of oxidation products was determined using DX-2700 X-ray diffraction (XRD) apparatus with Cu target. A glow discharge optical emission spectroscopy (GDOES) was used to identify the depth distribution of elements in the oxide scale.

## Results and Discussion

### Microstructure Characterization

The typical microstructures of the austenitic stainless steels containing Al and HR3C after solid solution treatment are presented in Fig. 1. It can be seen that all the matrix of the steels was composed of the single austenite phase grains. Besides that, a limited amount of bright spherical particles were randomly distributed in the grains and partially at grain boundaries (Fig. 1a). The particles were further analyzed by the energy-dispersive spectroscope (EDS), indicating that the participated phase of HR3C steel mainly consists of niobium and chromium elements (Fig. 1e). However, as shown in Fig. 1b–d, the black particles in austenitic stainless steels containing Al are mainly niobium-containing compounds (Fig. 1f), which were identified as the Nb-rich MX-type precipitation, termed as primary NbC [28–31].

### Oxidation Behavior

In order to understand the oxidation rate and chemistry, the isothermal oxidation of the alumina-forming austenitic steel and HR3C was performed. The specific weight

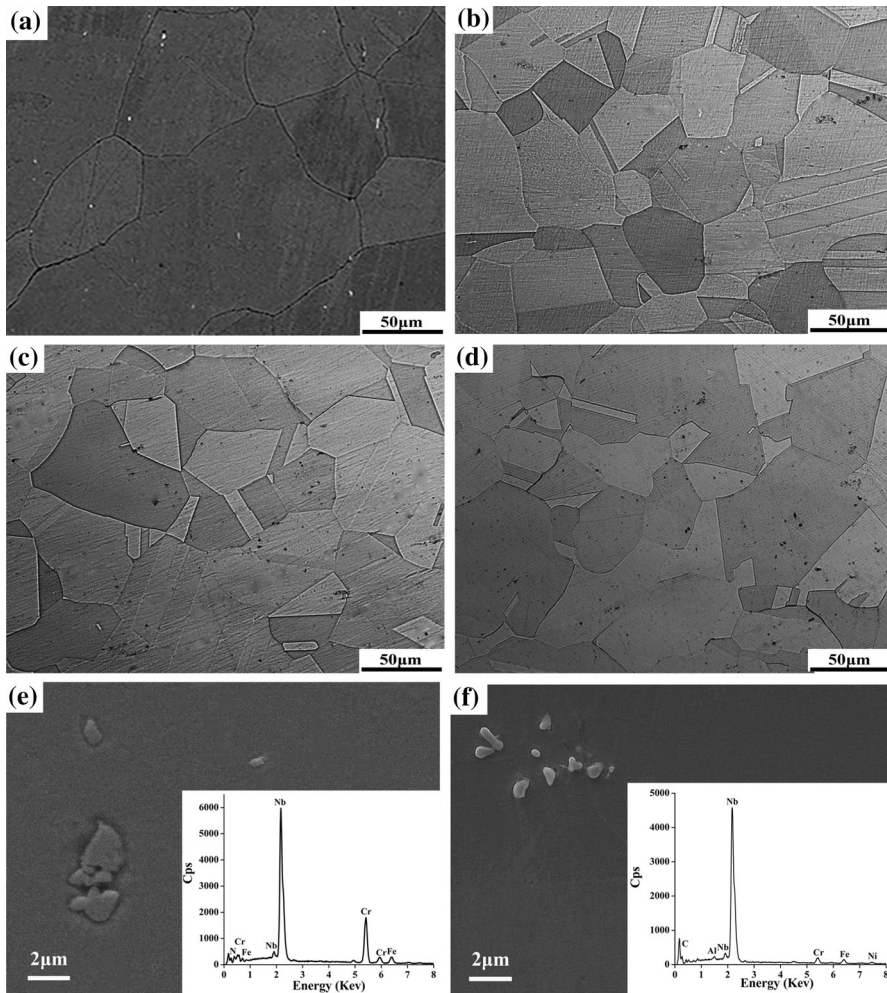


**Fig. 1** Microstructure after solution treatment of the alloys with various Al: **a** HR3C; **b** 22Cr–25Ni–1.5Al, **c** 22Cr–25Ni–2.5Al, **d** 22Cr–25Ni–3.5Al, and EDS spectrum corresponding to the precipitate in HR3C (**e**) and in alloys with Al (**f**)

change with time for samples tested at an approximately 800 °C isothermal hold in air is shown in Fig. 2. It is observed that the weight gain curve presents a parabolic law, indicating all these alloys exhibited good oxidation resistance, although the weight change is varied with the Al content. In the early oxidation process, the oxidation rate was rapid, which was caused by the chemical reaction between the oxygen and the specimen surface. Due to that the high Cr content promotes the diffusion of Cr in 22Cr–25Ni–1.5Al steels and HR3C, the oxidation rates of both steels were faster than of austenitic stainless steels with 2.5 and 3.5 wt% Al. However, the oxidation rate slowed down with the extension of the oxidation process, due to solid-state diffusion controlled reaction between the alloying

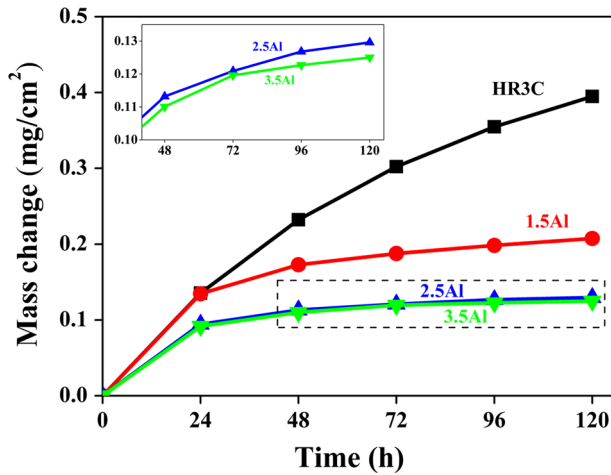


**Fig. 2** Kinetic curves of isothermal oxidation of the alloys with various Al contents at 800 °C in air

element through and the formed oxide film of the surface. The higher the Al content, the faster the oxidation rate decreased. Moreover, the HR3C steels showed the largest weight gain with the prolonged exposure time and reached up to  $0.4 \text{ mg cm}^{-2}$  after 120-h oxidation, but the weight gain in 22Cr–25Ni–1.5Al steel is reduced to  $0.23 \text{ mg cm}^{-2}$  after 120-h oxidation in dry air. When the Al content is at a relatively high level (above 2.5 wt% Al), the oxidation weight gain after 120 h of exposure maintains a lower level, not exceeding  $0.13 \text{ mg cm}^{-2}$ , suggesting a better oxidation resistance of these alloys.

Based on the analysis of oxidation kinetic curves, it is believed that different Al contents have great effects on surface morphologies and oxidation products on austenitic stainless steels. The SEM morphologies of oxide scales after isothermal oxidation at 800 °C in air for 120 h are presented in Fig. 3, and it shows that all the original surface of the steels is homogeneously oxidized.

For the HR3C steel, it can be seen from Fig. 3a that a scale consisting of loosely packed oxide particles was formed and the original grinding marks were invisible on the surface. Simultaneously, the interspacing of the grains is larger, which may act as the pathways for the transport of oxygen and alloy elements, leading to the serious oxidation. The higher magnifications (inset in Fig. 3a) were used to confirm the presence of large oxide grains in the oxidized surface. There are two main types of grains: One is a clavate structure with a diameter approximately  $4 \mu\text{m}$  (shown in Arrow 1), and the other is polycrystalline oxide structure with a relatively small size less than  $1 \mu\text{m}$  (shown in Arrow 2). According to the EDS analyses, both of the oxides are rich in Cr, Fe and Mn elements, suggesting the formation of Cr-containing oxides.

As to the steel with 1.5 wt% Al, the surface oxide scale exhibits a typical duplex oxide structure. The region marked with 3 in the inset of Fig. 3b mainly contained Cr, Mn, Fe and O elements, and the region marked with 4 contained Al, Cr, Fe and O elements in the EDS results. Based on the compositions of regions 3 and 4 and

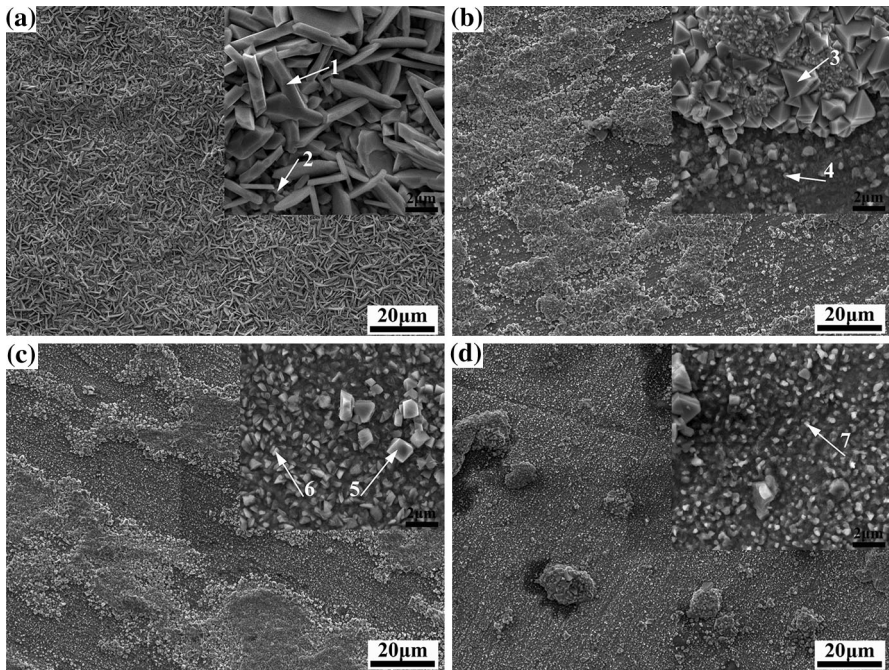


**Fig. 3** Surface morphology of the oxide scale on the alloys with various Al contents oxidized at 800 °C in air for 120 h: **a** HR3C, **b** 22Cr–25Ni–1.5Al, **c** 22Cr–25Ni–2.5Al, **d** 22Cr–25Ni–3.5Al. The insets in **a–d** are higher magnification images

their relative positions to each other, it is indicated that the formed oxidation films of the 22Cr–25Ni–1.5Al steel were composed by the outer Cr-containing oxide layer (region 3) and the inner Al-containing oxide layer (region 4) [32]. As the Al content increases, the EDS analysis shows that the amount of oxides concerning Cr, Mn and Fe has dwindled, but large amounts of oxides enriched in Al apparently increase. When the Al content increases to about 3.5 wt%, Fig. 3d shows that almost all of the oxides on the surface are rich in Al, and only occasional small amounts of Cr-rich, Mn-rich oxide surface nodules were observed. Moreover, the size of oxides formed on the Al-containing steels is finer than that of HR3C steel.

The corresponding XRD diffraction patterns of the oxides formed on the alloys are shown in Fig. 4. It is to be noted that the diffraction peaks of the austenite matrix appeared in the XRD spectrum with high intensity due to the fact that the oxide scale is thin. Figure 4a shows that  $\text{Cr}_2\text{O}_3$  has the strongest peak intensity among the phases of the HR3C steel, indicating the scale formed was quite thick. Besides, a trace amount of  $\text{FeCr}_2\text{O}_4$  phase was also found. As the aluminum contents are increased, the peak intensity of  $\text{Cr}_2\text{O}_3$  decreases and diffraction peaks corresponding to  $\text{Al}_2\text{O}_3$  started to appear. According to surface EDS from Table 2, the spinel structure in austenitic stainless steels containing Al was identified as  $\text{MnCr}_2\text{O}_4$  phase. Moreover, the intensity of  $\text{Al}_2\text{O}_3$  also increased with the Al content, indicating that the Al-rich oxide thinner oxide layer was formed.

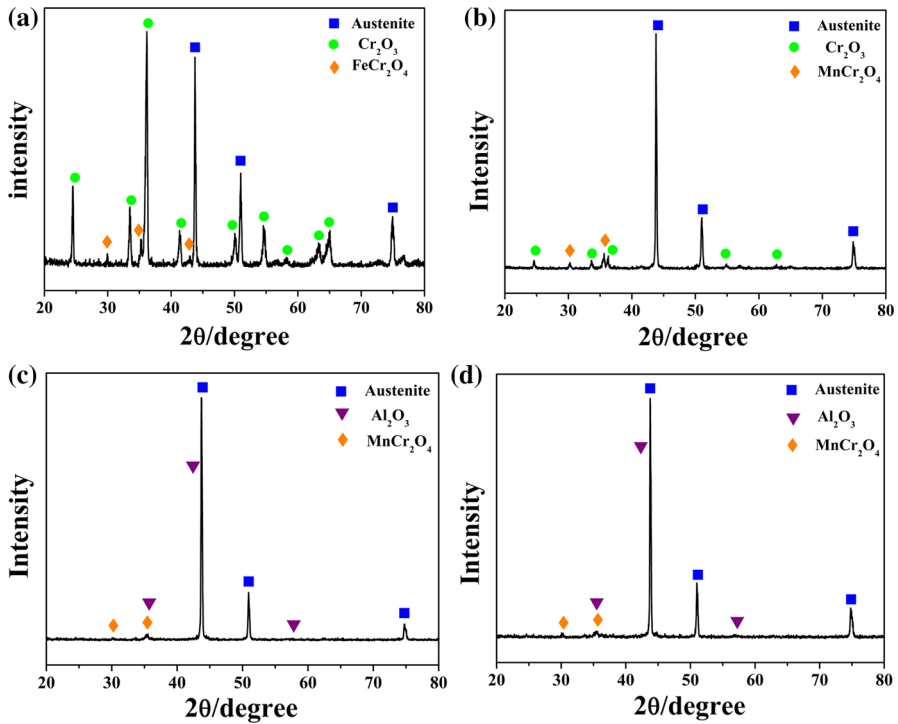


**Fig. 4** XRD patterns of the alloys oxidized for 120 h in air at 800 °C. **a** HR3C, **b** 22Cr–25Ni–1.5Al, **c** 22Cr–25Ni–2.5Al, **d** 22Cr–25Ni–3.5Al

**Table 2** EDS analyses of oxide films shown in Fig. 3

Area no.	Atom fraction/%					
	O	Fe	Cr	Ni	Mn	Al
1	58.9	10.0	26.9	0	4.2	–
2	61.6	6.8	28.6	0	3.0	–
3	55.5	5.0	26.7	2.5	10.3	0
4	48.9	7.5	13.2	4.2	2.2	24.0
5	56.5	5.2	23.3	3.5	11.5	0
6	59.6	0.8	3.4	0.5	0.6	35.1
7	56.5	1.0	2.9	2.3	0.9	36.4

### The Composition and Structure of Cross-Sectional Oxide Layer

It is obvious that the oxide scale formed on the austenitic stainless steels with higher Al contents is far more protective than that formed on the steels with lower Al contents, suggesting that the composition ( $\text{Cr}_2\text{O}_3$ - or  $\text{Al}_2\text{O}_3$ -rich oxide scale) and structure (multi-oxide layers or single oxide layer) of the oxide scales formed on the surface of the steels are different. Figure 5 shows cross-sectional SEM



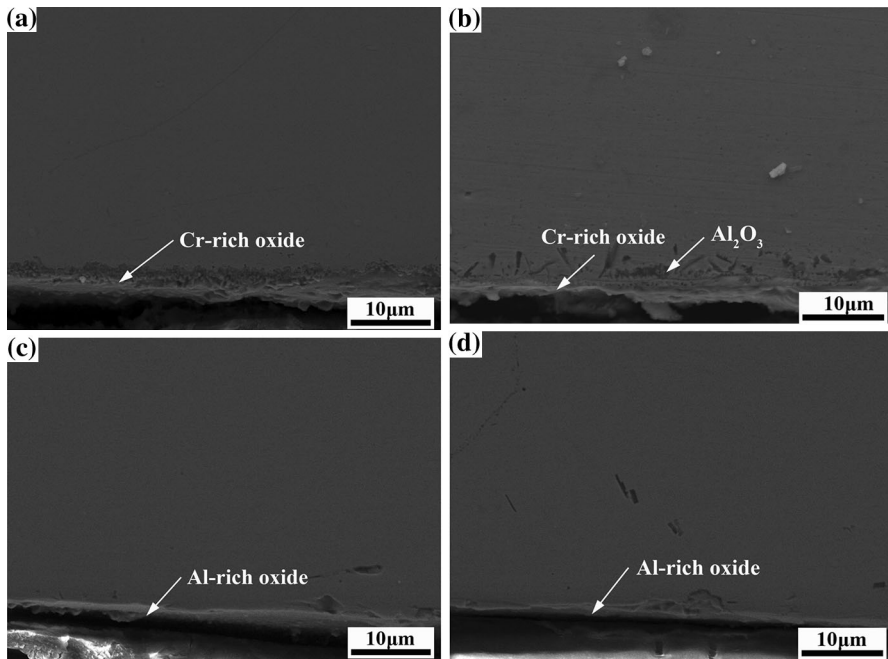


**Fig. 5** Cross-sectional morphology of the alloys oxidized at 800 °C. **a** HR3C, **b** 22Cr–25Ni–1.5Al, **c** 22Cr–25Ni–2.5Al, **d** 22Cr–25Ni–3.5Al

morphologies of the alloys oxidized at 800 °C in air for 120 h. It can be easily seen that the thickness of the oxide layer significantly decreases with the increase in aluminum content. As shown in Fig. 5a, the original HR3C alloy formed a much thicker and continuous oxide scale, along with a little internal oxidation. The scales formed on the austenitic stainless steels containing Al seem complicated. Figure 5b shows that the scale formed on 22Cr–25Ni–1.5Al (1.5 wt% Al) after oxidation was also extremely loose and thick. The corresponding SEM–EDS mapping images of Fig. 6a confirm that the layer mainly composed Cr- and O-rich oxide layer with a certain amount of subscale internal alumina. Nevertheless, with the increase in the Al content to 2.5 wt%, the inner oxidation is not as apparent as that of 22Cr–25Ni–1.5Al steel, and the cross-sectional oxidation morphology of Fig. 6b exhibited that a continuous and stable Al- and O-rich oxide layer was formed in the 22Cr–25Ni–2.5Al steel (Fig. 6b). The enrichment of Cr- or Fe-rich oxide in this surface layer is barely detectable, suggesting that the growth of scale was dominated by the outward Al diffusion. The similar phenomenon of Al- and O-rich oxide layer formed on the steel is also observed in Figs. 5d and 6c. Additionally, the oxide film formed on austenitic stainless steels containing 2.5 or 3.5 wt% Al (2 μm) is over twice thinner than that on HR3C (5 μm), which is consistent with the lesser weight gain in Fig. 2. Therefore, the addition of aluminum to austenitic stainless steels promotes the formation of a continuous Al- and O-rich oxide layer that may act as the diffusion barrier and improves the adhesion strength between the substrate and oxide scale,

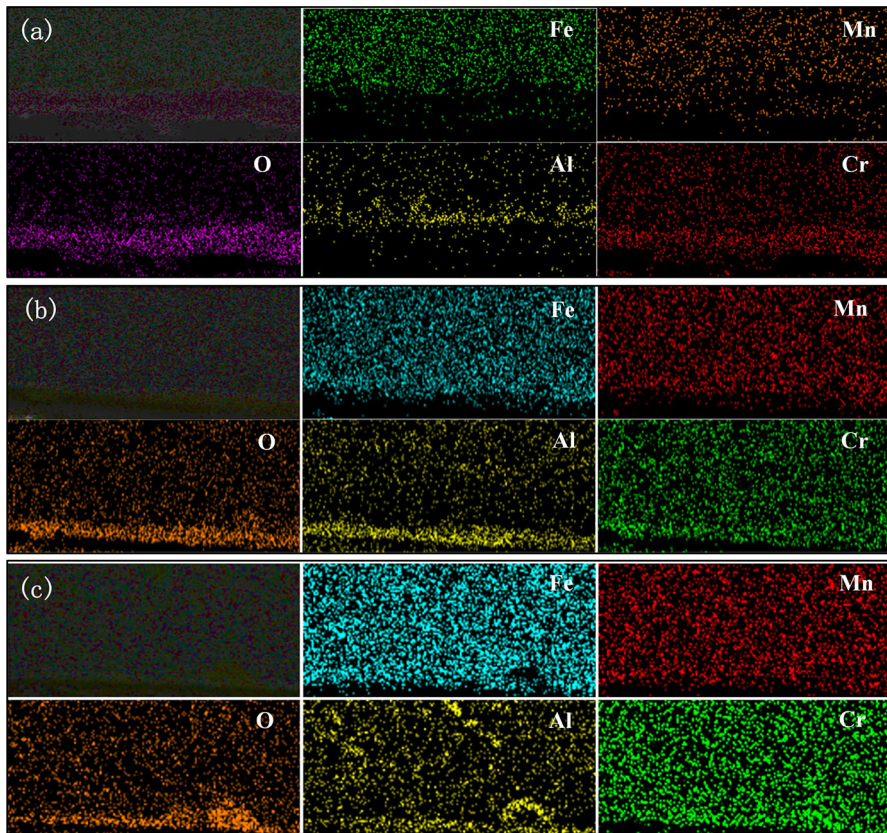


**Fig. 6** EDS mappings of the alloys oxide layers shown in Fig. 5. **a** 22Cr–25Ni–1.5Al, **b** 22Cr–25Ni–2.5Al, **c** 22Cr–25Ni–3.5Al

leading to a higher oxidation resistance of austenitic stainless steels containing Al than that of HR3C.

It can be speculated that increased aluminum content in the steels enhanced the oxidation resistance not only by fundamentally changing the type of scale formed, but also by modifying the scale morphology and layer structure.

In order to accurately analyze the formation mechanism of oxidation film and better understand the element distribution in-depth, the GDOES of the samples oxidized at 800 °C for 48 and 120 h from the matrix to the surface was analyzed, respectively. As shown in Fig. 7, the thickness of the oxide layers increases in all alloys with the time extended, but there are few changes in the composition and structure of oxide layer. Figure 7a shows the HR3C sample oxidized for 120 h mainly consists of Cr-rich oxide together with Fe- and Mn-rich oxide in the surface layer. Furthermore, the element depth distributions of Cr and Fe on surface are relatively wide, owing to the faster diffusion rate, which confirm the growth rate of oxide layers is greater. For this sample, the presence of a very thick oxide layer is corresponding to the XRD pattern before. However, the austenitic stainless steels

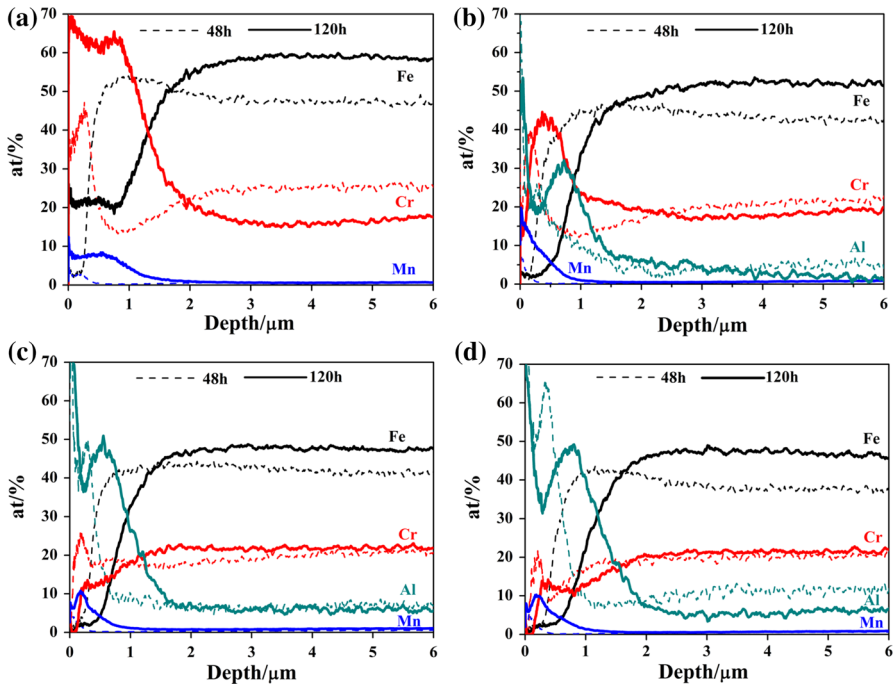


**Fig. 7** GDOES depth profiles of the alloys oxidized for 48 and 120 h in air. **a** HR3C, **b** 22Cr–25Ni–1.5Al, **c** 22Cr–25Ni–2.5Al, **d** 22Cr–25Ni–3.5Al. Dash line refers to oxidation for 48 h, and solid line refers to oxidation for 120 h

containing Al samples exhibit significant difference in the composition and structure at their surface compared with HR3C sample. The SEM analysis confirmed the 22Cr–25Ni–1.5Al steel has the continuous  $\text{Cr}_2\text{O}_3$  outer layer and the  $\text{Al}_2\text{O}_3$  inner layer structure. It can be clearly seen from Fig. 7b that the surface iron content significantly decreased compared with that of HR3C. The content peak of the aluminum element appeared between the outer Cr-rich oxide and the matrix. This is because the diffusion of Al element is slower than that of Cr, which results in the formation of internal alumina. For the 22Cr–25Ni–2.5Al and 22Cr–25Ni–3.5Al samples with more than 2.5 wt% Al, the oxide layers strongly enriched in aluminum and aluminum content at the highest point reaches around 50 at.%. It is shown from Fig. 7c that 22Cr–25Ni–2.5Al steel contains lower Cr and higher Al content compared with 22Cr–25Ni–1.5Al steel. Therefore, the increase in oxidation resistance of the steels is related to the higher Al content. According to the previous works [33, 34], the lattice distortion in alloys becomes more serious with the increased Al content, and consequently, the atomic movement is hindered and diffusion rate of element is reduced. The outer Cr oxide layer forms by outward diffusion of Cr across formed Al/Cr-mixed oxide layer. Therefore, the outward diffusion of Cr failed to develop on 22Cr–25Ni–2.5Al steel for 120-h oxidation because of the low diffusion rate of Cr, and only a mainly Al-rich oxide layer can be observed on the surface. In the other hand, it can be easily understood that Al-oxide

thin layer formed in the 22Cr–25Ni–2.5Al and 22Cr–25Ni–3.5Al steels can reduce the diffusion of Fe and Cr from inside the alloy to the outer side, which eventually makes the oxide scale thinner on the alloy's surface. Thus, the increase in Al concentration in the alloys is effective to reduce the oxide scale thickness.

### The Improvement Mechanism of Oxidation Resistance

The schematic mechanism of aluminum improving the oxidation-resistant property has been depicted in Fig. 8. The base alloy with no aluminum exhibited a continuous but not dense  $\text{Cr}_2\text{O}_3$  oxide layer. The growth mechanism of  $\text{Cr}_2\text{O}_3$  oxide scale is controlled not only by inward oxygen permeation from atmosphere, but also by outward chromium diffusion from the metallic substrate in HR3C austenitic stainless steel. The rough and loose oxide scales can easily lead to the high diffusion rate of oxygen through the oxide scale and the worse oxidation resistance property of stainless steels [23]. Figure 5a indicates that the formation of loose  $\text{Cr}_2\text{O}_3$  oxide layer leads to thicker oxide scales. Although the Cr element plays the most important role in protecting the HR3C alloy, the diffusion of Cr from inner to outer layers makes the depletion of chromium in inner region, which is shown by GDOES in Fig. 7a. When the aluminum content is in a low level (Fig. 8b), not only the oxide

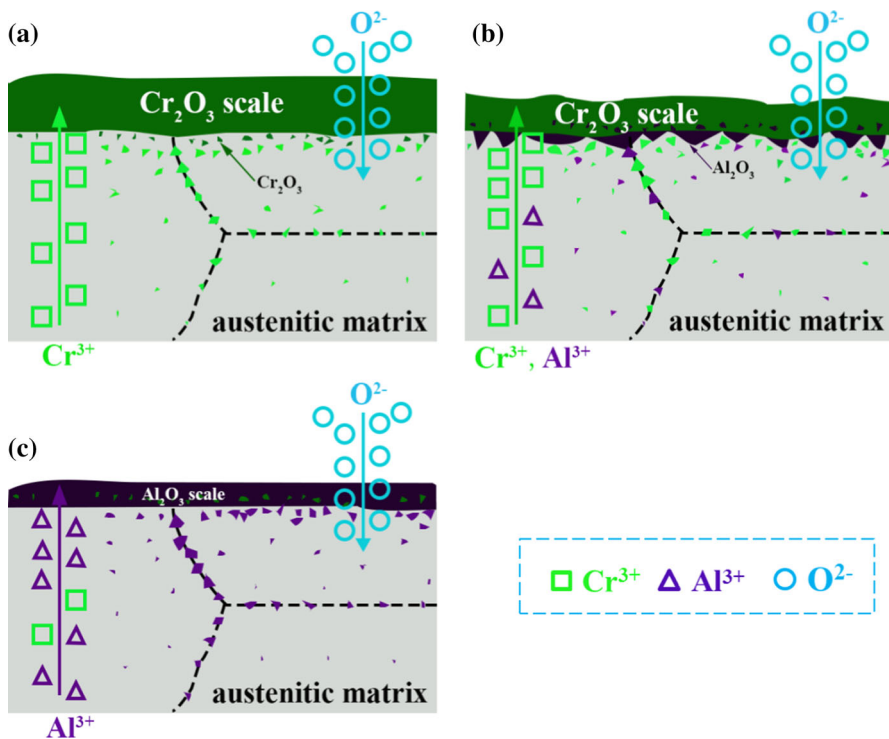


**Fig. 8** Schematic mechanism for the improved oxidation resistance of the AFA austenitic stainless steels oxidized at 800 °C in air: **a** in no aluminum contents, **b** in low aluminum contents and **c** in high aluminum contents

scale is very thick, but also the inner oxidation can easily occur by the formation of  $\text{Al}_2\text{O}_3$  oxide products (as shown in Fig. 5b). As for this case, the  $\text{Cr}_2\text{O}_3$  outer layer formed prior to the continuous  $\text{Al}_2\text{O}_3$  layer because of the both higher content of Cr with respect to Al and higher growth rate of  $\text{Cr}_2\text{O}_3$  compared with that of  $\text{Al}_2\text{O}_3$  [23].

When the aluminum content is in a higher level (Fig. 8c), the diffusion of Al is enhanced due to the increased aluminum content. Once the protective  $\text{Al}_2\text{O}_3$  layer has formed on the sample surface, the flux of oxygen from the outer layer to inner layer is decreased greatly and oxidation reaction of  $(4/3) \text{Al} + \text{O}_2 = (2/3) \text{Al}_2\text{O}_3$  is mainly controlled by transport of oxygen through the  $\text{Al}_2\text{O}_3$  layer. The activity of oxygen required to oxidize the Al is lower than that required to oxidize the Cr because Al- $\text{Al}_2\text{O}_3$  line lies lower than Cr- $\text{Cr}_2\text{O}_3$  line according to the Ellingham diagram [35]; therefore, the particles of  $\text{Al}_2\text{O}_3$  form in the outer layer prior to that of  $\text{Cr}_2\text{O}_3$  in steels with high aluminum contents. The formation of continuous and compact  $\text{Al}_2\text{O}_3$ -rich layer dramatically contributes to the improved oxidation resistance of austenitic stainless steels at high temperature. Therefore, alloying effects of aluminum on the oxidation behavior in this alloy merits investigation so that the anti-oxidation performance can be further optimized.

## Conclusions

In summary, the oxidation resistance of austenitic stainless steels modified with various aluminum contents was investigated.

The weight gain per unit area is in parabolic relation to oxidation time, and both the weight gain and the thickness of the oxide scale significantly decrease with increased aluminum contents.

1. Addition of aluminum into austenitic stainless steels changes phase composition and density of the oxide film. Surface oxides of austenitic stainless steel transform from  $\text{Cr}_2\text{O}_3$  to a composite oxide layer comprising Cr and Al. When the aluminum content is in a higher level, the oxides enriched in Al are dominant and the oxides film is more compact.
2. Compared with the oxide film on HR3C, thinner oxide films with smaller size of oxide particles are realized on 22Cr–25Ni–2.5Al and 22Cr–25Ni–3.5Al steels, indicating a superior oxidation resistance of both steels to HR3C steel.
3. With the increase in aluminum content, the diffusion of Al is enhanced and protective  $\text{Al}_2\text{O}_3$  scale in austenitic stainless steels was formed via adjusting the relative content of Cr and Al.  $\text{Al}_2\text{O}_3$  is more compact oxide film than  $\text{Cr}_2\text{O}_3$ , which hinders the further oxidation of alloys and significantly improves the oxidation resistance of alloys at high temperature.

**Acknowledgements** This research was supported by the National Natural Science Foundation of China (Grant No. 51371123), the National Natural Science Foundation of Shanxi province (Grant No. 2014011002), the Research Fund for the Doctoral Program of Higher Education of China (20131402110003) and Shanxi Province Science Foundation for Youths (201601D202033).

## References

1. D. P. Hanak, C. Biliyok and V. Manovic, *Applied Energy* **151**, 2015 (258).
2. R. Mikulandrić, D. Lončar, D. Cvetinović and G. Spiridon, *Energy* **57**, 2013 (55).
3. D. Pudasainee, J. H. Kim, S. H. Lee, J. M. Park, H. N. Jang, G. J. Song and Y. C. Seo, *Asia-Pacific Journal of Chemical Engineering* **5**, 2010 (299).
4. F. Lin, S. Cheng and X. Xie, *Energy Materials Materials Science & Engineering for Energy Systems* **3**, 2008 (201).
5. F. Masuyama, *ISIJ International* **41**, 2001 (612).
6. R. Viswanathan, R. Purgert, S. Goodstine, J. Tanzosh, G. Stanko, J. P. Shingledecker, and B. Vitalis, *International Conference on Advances in Materials Technology*, Vol. 1 (2008).
7. R. Viswanathan, K. Coleman and U. Rao, *International Journal of Pressure Vessels & Piping* **83**, 2006 (778).
8. J. C. Rosser, M. I. Bass, C. Cooper, T. Lant, P. D. Brown, B. J. Connolly and H. E. Evans, *Materials at High Temperatures* **29**, 2012 (95).
9. J. Jianmin, M. Montgomery, O. H. Larsen and S. A. Jensen, *Materials & Corrosion* **56**, 2005 (542).
10. T. Dudziak, M. Łukaszewicz, N. Simms and J. R. Nicholls, *Corrosion Engineering Science and Technology* **50**, 2015 (272).
11. J. Fu, N. Li, Q. Zhou and P. Guo, *Oxidation of Metals* **83**, 2015 (317).
12. J. Yan, Y. Gu, F. Sun, Y. Xu, Y. Yuan, J. Lu, Z. Yang and Y. Dang, *Materials Science and Engineering A* **675**, 2016 (289).
13. E. J. Opila, *Materials Science Forum* **461**, 2004 (765).
14. H. Asteman, J. E. Svensson, M. Norell and L. G. Johansson, *Oxidation of Metals* **54**, 2000 (11).
15. H. Asteman, J. E. Svensson and L. G. Johansson, *Corrosion Science* **44**, 2002 (2635).
16. S. R. J. Saunders, M. Monteiro and F. Rizzo, *Progress in Materials Science* **53**, 2008 (775).
17. J. Yuan, W. Wang, H. Zhang, L. Zhu, S. Zhu and F. Wang, *Corrosion Science* **109**, 2016 (36).
18. M. P. Brady, Y. Yamamoto, M. L. Santella, P. J. Maziasz, B. A. Pint, C. T. Liu, Z. P. Lu and H. Bei, *JOM-Journal of Metals Minerals, and Material Society* **60**, 2008 (12).
19. Y. F. Yan, X. Q. Xu, D. Q. Zhou, H. Wang, Y. Wu, X. J. Liu and Z. P. Lu, *Corrosion Science* **77**, 2013 (202).
20. D. W. Yun, S. M. Seo, H. W. Jeong and Y. S. Yoo, *Corrosion Science* **83**, 2014 (176).
21. X. Zhang, L. Fan, Y. Xu, J. Li, X. Xiao and L. Jiang, *Materials and Design* **65**, 2015 (682).
22. S. Tang, S. Zhu, X. Tang, H. Pan, X. Chen and Z. D. Xiang, *Corrosion Science* **80**, 2014 (374).
23. Y. Xu, X. Zhang, L. Fan, J. Li, X. Yu, X. Xiao and L. Jiang, *Corrosion Science* **100**, 2015 (311).
24. Y. Yamamoto, M. P. Brady, Z. P. Lu, P. J. Maziasz, C. T. Liu, B. A. Pint, K. L. More, H. M. Meyer and E. A. Payzant, *Science* **316**, 2007 (433).
25. X. Xu, X. Zhang, G. Chen and Z. Lu, *Materials Letters* **65**, 2011 (3285).
26. X. Xu, X. Zhang, X. Sun and Z. Lu, *Corrosion Science* **65**, 2012 (317).
27. J. Wang, Z. Liu, H. Bao and S. Cheng, *Journal of Iron and Steel Research International* **20**, 2013 (113).
28. J. Jiang and L. Zhu, *Materials Science & Engineering A* **539**, 2012 (170).
29. D. Q. Zhou, W. X. Zhao, H. H. Mao, Y. X. Hu, X. Q. Xu, X. Y. Sun and Z. P. Lu, *Materials Science & Engineering A* **622**, 2015 (91).
30. C. Chi, H. Yu, J. Dong, W. Liu, S. Cheng, Z. Liu and X. Xie, *Progress in Natural Science: Materials International* **22**, 2012 (175).
31. V. T. Ha and W. S. Jung, *Materials Science & Engineering A* **558**, 2012 (103).
32. X. Chen, J. F. Stubbins, P. Hosemann and A. M. Bolind, *Journal of Nuclear Materials* **398**, 2010 (172).
33. P. K. Huang, J. W. Yeh, T. T. Shun and S. K. Chen, *Advanced Engineering Materials* **6**, 2004 (74).
34. F. J. Wang, Y. Zhang and G. L. Chen, *Journal of Alloys & Compounds* **478**, 2009 (321).
35. M. Hasegawa, *Chapter 3.3—Ellingham Diagram Treatise on Process Metallurgy: Process Fundamentals*, Vol. 1 (2014), p. 507.